Journal of Interfaces, Thin films, and Low dimensional systems 5 (2) Winter and Spring (2022) 479-492

Investigation of Zr nanoparticle effects on structural phase stability, micro strains, and flux pinning in BSCCO-Zr/Cu doped HTSC

Scientific research paper

Sadaf Vafajoo, Vahid Daadmehr*, Fatemeh Shahbaz Tehrani

Magnet&Superconducting Research Lab., Faculty of Physics, Alzahra University, Tehran 19938, Iran

ARTICLE INFO

Article history:
Received 11 December 2022
Revised 31 January 2023
Accepted 8 February 2023
Available online 13 April 2023

Keywords
High-Temperature Superconductivity
Sol-gel processes
Flux pining and creep
X-ray diffraction
Zr nanoparticle
BSCCO-Zr/Cu

ABSTRACT

In this research, the resistivity of the $Bi_{1.66}Pb_{0.34}Sr_2Ca_2Cu_{3-x}Zr_xO_{10+\delta}$ (Bi-2223) polycrystalline samples (x=0.0, 0.002, 0.0075, and 0.01) synthesized by the sol-gel method, has been investigated under magnetic fields. Also, the structural and morphological properties of ceramic superconductors have been studied by using X-ray diffraction (XRD) and Field Emission Scanning Electron Microscopy (FESEM) measurements. It is found that the Bi-2223 structural phase was formed more than other phases in the synthesized samples for $x \leq 0.0075$. Based on the resistivity measurements, it is understood that the T_C decreases with the increase in the Zr doping and the second superconducting transition is seen for the $x \geq 0.0075$. The thermally activated flux creep (TAFC) model has been investigated in synthesized ceramic superconductors. Furthermore, the magneto resistivity behavior of all samples has been analyzed to determine the dependence of the pinning energy with applied magnetic fields and Zr doping. It is found that the pinning energy remarkably decreases with rise of the Zr doping. Therefore, the creeping of vortices and crossing the energy barrier occur more easily, thus the pinning energy is reduced by increasing the Zr doping. Moreover, a good agreement between the modified TAFC model and the experimental data is concluded for the synthesized compounds.

1 Introduction

The study of high-temperature superconductors (HTSC) has attracted the attention of scientists due to their wide technological applications and different physical properties. In comparison to conventional superconductors, these differences are related to the high transition temperature (T_C), high critical current density (J_C), new electronic structure, and flux dynamics [1-5]. Bismuth Strontium Calcium Copper Oxide (BSCCO) superconductors as a group of HTSC from the cuprates family have different compositions depending on the different numbers of CuO_2 planes. BSCCO superconductors have a common formula $(Bi, Pb)_2Sr_2Ca_{n-1}Cu_nO_{2n+4+\delta}$,, where n shows the number of CuO_2 planes in the unit cell. Due to the different number of CuO_2, the T_C changes in the BSCCO superconductors (T_C~20 K for n=1 (Bi-2201) [6], T_C~85 K for n=2 (Bi-2212) [7], and T_C~110 K for n=3 (Bi-2223) [8-10]). Among the mentioned structural phases, the Bi-2223 is the most favorable phase for the processing of tapes, wires, and then energy storage for high-current applications [11-14]. However, the preparation of a perfectly pure Bi-2223 polycrystalline superconductor is difficult because several undesirable phases such as Bi-2212, Bi-2201, and Sr_2CuO_3 are

*Corresponding author.
Email address: daadmehr@alzahra.ac.ir
DOI: 10.22051/jitl.2023.42264.1076

usually created in the synthesized superconductor [15-17]. The creation of weak links is the most important effect of undesirable secondary phases and as a result the restriction in the usage of the Bi-2223 superconductor for industrial applications. In the literature, the impacts of heat treatment and nano-size dopants and additives on the decline of impurity phases in Bi-2223 superconductors have been studied. It has been shown that by modifying the process parameters and choosing the optimum added and dopant values, the Tc and Jc values can be improved [18-20]. Also, it was determined that the impurity phases had placed between Bi-2223 grains, and as undesirable secondary phases were reduced in the synthesized Bi-2223 superconductor, the Tc and Jc improved [18-21].

Up to now, the substitution of various doping has been studied by many researchers, and the superconductivity properties of the synthesized ceramics have been investigated [22-25]. The substitution of Pb in the site of Bi can improve the volume percent of the Bi-2223 phase, and so the superconducting onset temperature (T_C^{onset}) increases [26, 27]. Also, the addition of ZrO_2 nanoparticles to the BSCCO ceramic superconductors decreased the T_C onset, but the J_C enhanced under magnetic fields [28]. It can be attributed to the presence of the flux pinning that has been created by the ZrO_2 nanoparticles. Furthermore, Zouaoui et al. studied the effects of nanoparticles ZrO_2 addition on the flux pinning properties of (Pb, Bi)-2223 superconductor and found that the activation energies of the vortex flux motion, J_C, and the volume density of pinning force increase for 0.1 wt.% ZrO_2 sample [29]. Additionally, the heat treatments and the role of the 'additive' ZrO_2 on the superconductivity properties of Bi-2223 compounds had been investigated by Azhan et al. [30]. However, from the point of view of the strength of structural phases, the substitution effects of zirconium ions in the sites of various elements of BSCCO ceramic superconductors such as copper, bismuth, etc are extremely rare, and it is still an open issue. Consequently, we choose it for our research and investigate the substitution impact of Zr/Cu doping on the volume percent of the Bi-2223 and undesirable secondary phases and as well as the superconductivity parameters.

Among the transport investigations, the response of the superconductivity parameters to the magnetic field is one of the interesting studies [31-33]. The magnetic field causes the broadening of electrical resistivity (ρ) in the superconductivity transition region [34]. The region of the broadening is divided into the intergrain and intragrain regions. Due to the fluctuations of the superconductivity order parameters, there are different models for the study of the broadening of ρ in the magnetic field such as flux creep [35], flux flow [36, 37], and phase slip models [38]. The thermally activated flux creep (TAFC) model is the appropriate approach for the study of the flux lattice motion in the magnetic field [39, 40]. Some research groups have illustrated that this model can describe the temperature broadening of ρ near T_C (ρ=0) [40]. But, the studies about the flux dynamics for various substitutions are continued.

With this background, in this paper, we investigate the substitution effects of Zr/Cu nanoparticle doping on the (Pb, Bi)-2223 ceramic superconductors synthesized by the sol-gel method, for these purposes: i) The competition for the formation of structural phases of BSCCO with the Zr doping, ii) The effects of Zr/Cu substitution on structural micro strain, iii) investigation of morphological properties, iv) study of superconductivity parameters by Zr/Cu substitution on BSCCO+Zr, and Finally, we study the magneto resistivity and the flux dynamics by using the modified TAFC model.

2 Experimental method, chemicals and characterization with measurement system

There are several chemical methods for the synthesis of HTSC [41-44] where the sol-gel method is one of the best. This procedure is widely used because of its lower preparation temperature, better homogeneity, repeatability, lower unwanted phases, etc. Therefore, in our experiment, the $Bi1.66Pb0.34Sr2Ca2Cu3-xZrxO10+\delta$ ceramics with x=0.0, 0.002, 0.0075, and 0.01 where synthesized by this method. We utilized $Bi(NO_3)_3.5H_2O$ (99.9%), $Pb(NO_3)_2$ (99.9%), $Sr(NO_3)_2$ (99.9%), $Ca(NO_3)_2.4H_2O$ (99%), $Cu(NO_3)_2.3H_2O$ (99%), and ZrO_2 (99.9%) as raw materials. The stoichiometric amount of bismuth nitrate was dissolved in 20 ml of deionized water and stirred at 50°C. Then we added nitric acid to form a clear solution and avoid the formation of $Bi(OH)_2NO_3$. Then the other nitrates and ZrO_2 were dissolved in this solution separately which was stirred at 50°C to obtain the precursor

solution with blue color. For the formation of the base solution, polyethylene glycol (PEG) was added to 20 ml of the deionized water which was stirred at 50°C. Then ethylenediaminetetraacetic acid (EDTA) in which the molar ratio of EDTA to the total metal ions is 1:1 was added gradually to the solution. Ammonia was added to the solution for increasing solubility. Afterward, EDTA was completely dissolved in the PEG solution and a clear colorless solution was obtained. The pH of the base solution was measured and it was one. At this stage, the base solution was formed and then the solution of the nitrates was added to the base solution by a separator funnel. At this step, with adding the solution of the nitrates to the base solution, some ammonia was added for better dissolving of materials. Finally, the dark blue solution was formed. Then Urea was added to the solution as a preservative and the sol was heated continuously at 80°C under stirring to form a brown gel. The gel was heated in an oil bath at 120°C for 10 hours, and then at 180-250°C for 8 hours. The gel fired at 220-250°C and formed a black foam-like mass. The obtained material was grounded into powder for 2 hours and was calcined at 800°C for 30 hours, and repeated. After calcination, the obtained powder was grounded and pressed into the pellets with a 10 mm diameter. Finally, the pellets were sintered at 835°C for 200 hours.

The X-ray diffraction (XRD) patterns of the samples were obtained by using a PANalytical® PW3050/60 X-ray diffractometer with Cu Kα radiation (λ= 1.54056 Å) operated at 40 kV and 40 mA with a step size of 0.026°. The refinement method of Rietveld was applied with the "Material Analysis Using Diffraction" (MAUD) software (v.2.8). A Tescan®–Vega3 Field Emission Scanning Electron Microscope (FE-SEM) was applied for the morphology investigation of the synthesized samples. A four-probe technique for the superconductivity measurements was performed using the 20K Closed Cycle Cryostat (QCS101), ZSP Cryogenics Technology. Also, we applied a Lake Shore-325 temperature controller for measuring the temperature and the DC (Lake Shore-120) was 10 mA. Likewise, the voltage was measured with microvolt accuracy.

3. Results and discussion

3.1 Structural investigations

The XRD patterns of the synthesized samples for Zr doping are shown in Figure 1. For the BSCCO+Zr (x=0.002) sample, Figure 2 shows the refinement results by the MAUD software. The Bi-2223 phase with the orthorhombic structure and with (A2aa:cab) group symmetry exists as a dominant phase. Also, the Bi-2212 and Sr_2CuO_3 structural phases are formed in this sample.

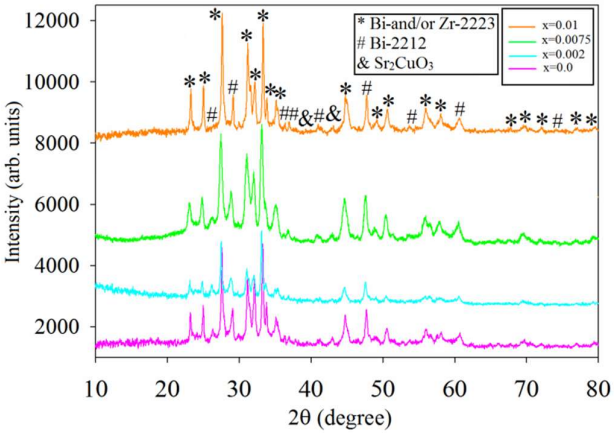

Figure 1. The XRD patterns of the synthesized samples for the Zr doping

According to the MAUD results, the volume percent of the mentioned phases for different Zr doping is investigated and listed in Table 1. As shown in Table 1, with the substitution of the Zr/Cu ions, the Zr ions are preferably placed in the Bi-2223 phase which is labeled as the Bi-2223+Zr phase. The refined values (such as occupancy number, atomic positions, etc.) for the Bi-2223+Zr phase are presented in Table 2. The agreement of the real- and experimental values of Zr and Cu occupancy numbers indicates that the substitution of Zr/Cu ions completely occurs on the CuO_2 planes. Also, based on the results in Table 1, by increasing the Zr doping up to 0.0075, the volume percent of the Bi-2223+Zr phase increases, and the Bi-2212 phase decreases so that for x=0.0075, the Bi-2212 phase never forms. Furthermore, the undesirable Sr_2CuO_3 phase decreases, and so, the Zr doping causes the stability of the Bi-2223 phase and decreasing of the undesirable phases in the synthesized samples.

Table 1. The volume fraction (%), lattice parameters and orthorombicity for synthesized samples

Zr content (x)	Vol. %. of phases				
	Bi-2223	Bi-2212	Sr_2CuO_3	Bi-2223+Zr	Bi-2212+Zr
0	70.8	15.4	13.8	-	-
0.002	26.2	0.0	5.6	68.2	0.0
0.0075	17.6	0.0	3.1	69.3	10.0
0.01	20.2	20.7	16.6	28.5	14.0

Zr content (x)	Lattice parameters For Bi-2223 phase			Lattice parameters For Bi-2223+Zr phase		
	a (Å)	b (Å)	c(Å)	a (Å)	b (Å)	c(Å)
0	5.406	5.404	37.347	-	-	-
0.002	5.403	5.404	37.049	5.713	5.807	38.86
0.0075	5.403	5.403	37.002	5.702	5.788	38.79
0.01	5.402	5.419	36.957	5.587	5.512	38.70

Zr content (x)	Orthorombicity for Bi-2223 phase/Sample (%)	Orthorombicity for Bi-2223+Zr phase/Sample (%)
0	0.02	-
0.002	0	0.82
0.0075	0	0.75
0.01	0.16	0.68

Consequently, it can be proposed that a small amount of Zr/Cu substitution ($x \leq 0.0075$) can be helpful to form the Bi-2223 phase completely and remove the undesirable secondary phases in Bi-2223 superconductors. So as an applicable result, it can be used in the processing of tapes, wires, and energy storage for high-current applications. Table1 shows that with the increase of the Zr content for x=0.01, the Bi-2212 phase forms again, and also the volume percent of the Sr_2CuO_3 phase increases in the synthesized samples. This issue is confirmed by the resistivity measurement results described in the next sections.

Figure 2 shows the experimental and calculated XRD patterns that have been refined with the MAUD software for the x=0.002 doping. The fitness quality can be examined for XRD data by the calculation of the fit goodness (S). It is calculated by $S= R_{wp} /R_{exp}$, where R_{wp} is the weighted residual error and R_{exp} is the expected error. The best refinement is obtained when S is close to 1. These parameters for the synthesized compounds are registered in Table 3 and show good refinements.

Table 2. The refined values of atomic positions and occupancy calculated from the MAUD software for the Bi-2223+Zr phase in the synthesized compounds

Zr doping x=0.0					Zr doping x=0.002			
Atoms	x	y	z	*occupancy*	x	y	z	*occupancy*
Bi	0.0	0.0	0.21	0.8	0.0	0.0	0.21	0.8
pb	0.0	0.0	0.21	0.2	0.0	0.0	0.21	0.2
Sr	0.0	0.0	0.35	1.0	0.0	0.0	0.35	1.0
Ca	0.0	0.0	0.46	1.0	0.0	0.0	0.46	1.0
Cu(1)	0.0	0.0	0.0	1.0	0.0	0.0	0.0	0.998
Cu(2)	0.0	0.0	0.09	1.0	0.0	0.0	0.09	1.0
O(1)	0.0	0.5	0.0	1.0	0.0	0.5	0.0	1.0
O(2)	0.0	0.5	0.09	1.0	0.0	0.5	0.09	1.0
O(3)	0.0	0.0	0.15	1.0	0.0	0.0	0.15	1.0
O(4)	0.0	0.0	0.29	1.0	0.0	0.0	0.29	1.0
Zr	-	-	-	-	0.0	0.0	0.0	0.0018
Zr doping x=0.00.75					Zr doping x=0.01			
Atoms	x	y	z	*occupancy*	x	y	z	*occupancy*
Bi	0.0	0.0	0.21	0.8	0.0	0.0	0.21	0.8
pb	0.0	0.0	0.21	0.2	0.0	0.0	0.21	0.2
Sr	0.0	0.0	0.35	1.0	0.0	0.0	0.35	1.0
Ca	0.0	0.0	0.46	1.0	0.0	0.0	0.46	1.0
Cu(1)	0.0	0.0	0.0	0.992	0.0	0.0	0.0	0.990
Cu(2)	0.0	0.0	0.09	1.0	0.0	0.0	0.09	1.0
O(1)	0.0	0.5	0.0	1.0	0.0	0.5	0.0	1.0
O(2)	0.0	0.5	0.09	1.0	0.0	0.5	0.09	1.0
O(3)	0.0	0.0	0.15	1.0	0.0	0.0	0.15	1.0
O(4)	0.0	0.0	0.29	1.0	0.0	0.0	0.29	1.0
Zr	0.0	0.0	0.0	0.0073	0.0	0.0	0.0	0.010

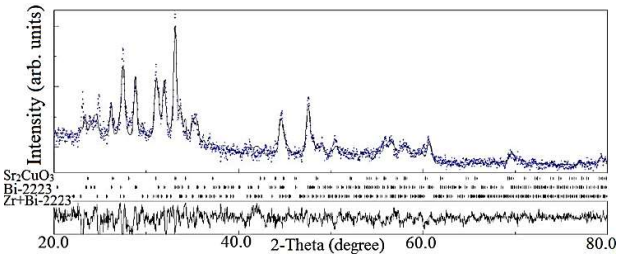

Figure 2. The XRD pattern of x=0.002 compound that is refined by the MAUD software.

Table 3. The refinement parameters computed by the MAUD software, Williamson-Hall equation, microstrain, and crystallite size for the Zr doping.

Zr content (x)	R_{wp}(%)	R_{exp} (%)	R_b (%)	S
0	4.663	2.395	3.628	1.95
0.002	6.840	4.111	3.225	1.66
0.0075	6.419	3.546	3.762	1.81
0.01	6.208	3.848	3.375	1.61

Zr content (x)	Williamson-Hall equation	Microstrainη(%)	Crystallite size D (nm)
0	y=0.003x+0.015	0.3±0.02	66.67±0.03
0.002	y=0.008x+0.011	0.8±0.01	90.91±0.05
0.0075	y=0.007x+0.011	0.7±0.04	90.93±0.04
0.01	y=0.005x+0.009	0.5±0.04	111.11±0.05

Based on the MAUD results, the lattice parameters for the Bi-2223 and Bi-2223+Zr phases have been calculated for Zr doping and are listed in Table 1. It is seen that by the substitution of Zr/Cu ions up to x=0.002, the lattice parameters of Bi-2223+Zr increase compared to the undoped sample (Bi-2223 phase). Also, with more increase in the Zr doping, the lattice parameter "c" of Bi-2223+Zr declines. The decrease of the lattice parameter "c" may be attributed to the increase in the attraction between layers with the increase of Zr doping. The reduction of the lattice parameter "c" will be confirmed by resistance measurements and the decrease of T_C. Furthermore, the lattice parameter "c" of the Bi-2223 phase decreases with the rise of the Zr doping. Additionally, the orthorombicity percent has been attained through the following formula for the Bi-2223 and Bi-2223+Zr structural phases and listed in Table 1.

$$Orthorombicity(\%) = 100\frac{(b-a)}{(b+a)}. \quad (1)$$

As shown in Table 1, the orthorombicity of the Bi-2223+Zr phase increases up to x=0.002 compared to the Bi-2223 phase and then decreases by a further increase of Zr doping for other ones. The variation of lattice parameters "a" and "b" (and the orthorombicity) with increasing the Zr doping up to x=0.002 can be explained by the following reasons: i) The atomic shells of Zr ions are more than Cu ions, ii) The symmetry breaking occurs for the CuO_2 planes due to the gradual substitution of Zr/Cu ions (Figure 3 shows schematically this issue). Also, with more substitution of Zr/Cu ions in each CuO_2 plane up to x = 0.01, a new symmetry may create for the CuO_2 plane and so the lattice constants decrease and then the orthorombicity decreases (see Figure 3). These phenomena can be attributed to the electron affinity of Zr ions in comparison to Cu ions.

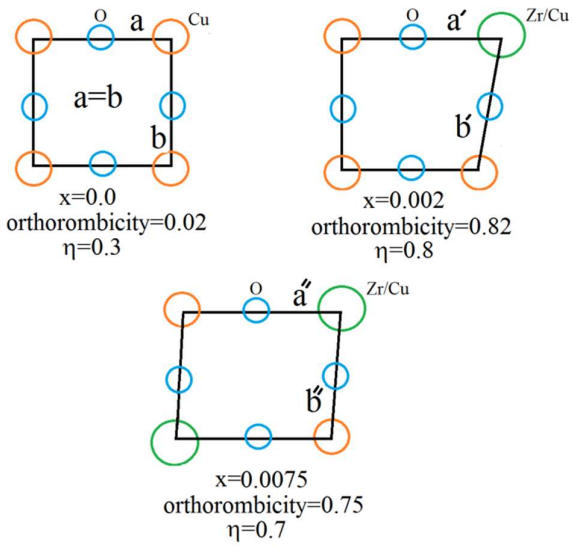

Figure 3. The schematic picture of a CuO_2 plane for the synthesized samples.

According to the above process, the variations of the lattice parameters with the increase in the Zr doping can affect the creation of microstrains in the synthesized samples. To investigate this issue, the microstrain η and crystallite size D can be calculated through Williamson–Hall equation for the synthesized samples:

$$\frac{\beta\, cos\theta}{\lambda} = \frac{K}{D} + \frac{\eta\, sin\theta}{\lambda}, \quad (2)$$

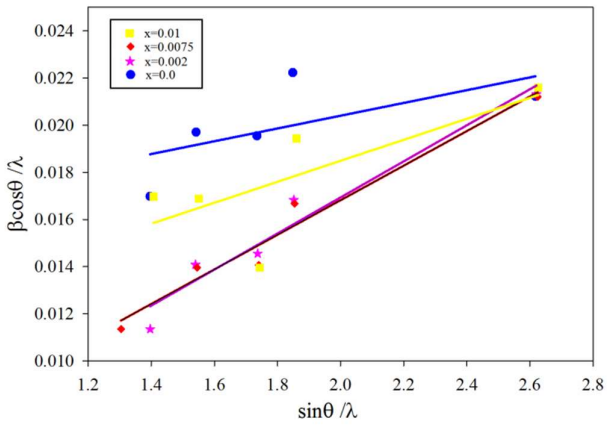

Figure 4. Williamson–Hall plot of the synthesized samples for the Zr doping.

where K is Scherer's constant, β and θ are full width at half maximum (FWHM) and diffraction angle for each peak, respectively [45]. Figure 4 shows Williamson-Hall plots for the synthesized samples, and the calculated microstrain while the average crystallite sizes are listed in Table 3. It is seen that with increasing the Zr doping in the synthesized samples, as the orthorombicity first increases and then decreases, the microstrains undergone a similar process. In other words, the fluctuations of microstrains are consistent with orthorombicity variations with the Zr/Cu substitution while the changes in microstrains indicate a gradual occupation and change in the symmetry of the CuO_2 planes. In addition, the microstrains have the same order of magnitude for all synthesized samples.

3.2 Morphological study

Figures 5a, b, and c display the images of FE-SEM for x=0.0, 0.0075, and 0.01 compounds. It is understood that all samples have a granular structure and oriented grains in random directions. Also, the Zr doping has not clearly influenced the morphology of the doped samples such as connectivity, defects, orientation, and porosity.

3.3 Electrical measurements

The temperature dependence of the normalized electrical resistivity for the Zr doping is presented in Figure 6. The T_C^{onset}, T_C^{mid}, and T_C^{offset} of each superconductivity phase has been defined as the temperatures where the resistivity drops 10%, 50%, and 90% from its earlier state value, respectively. It should be noticed that the earlier state is the normal state for the Bi-2223 and/or Bi-2223+Zr phases and is the

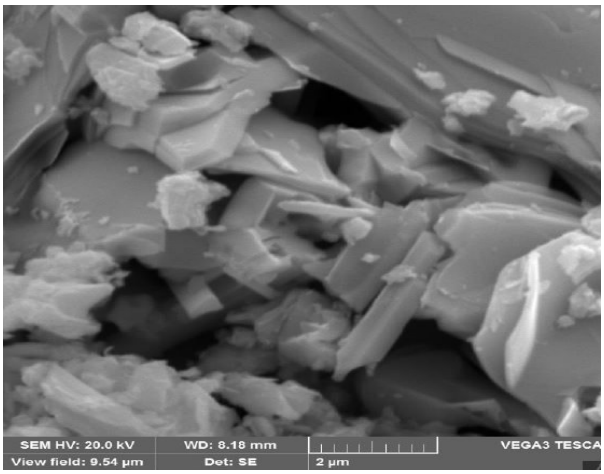

Figure 5a. The FE-SEM image for x=0.0 synthesized sample.

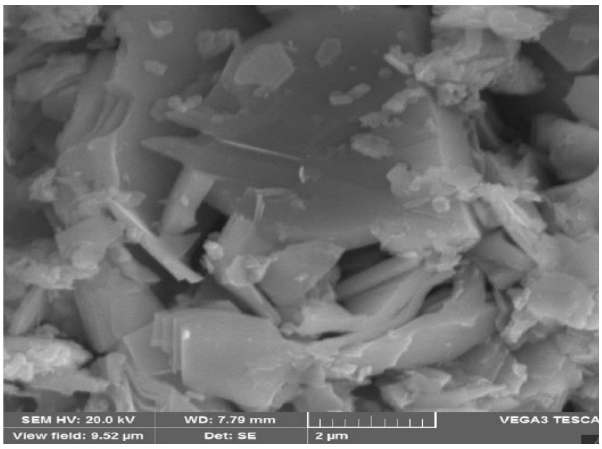

Figure 5b. The FE-SEM image for x=0.0075 synthesized sample.

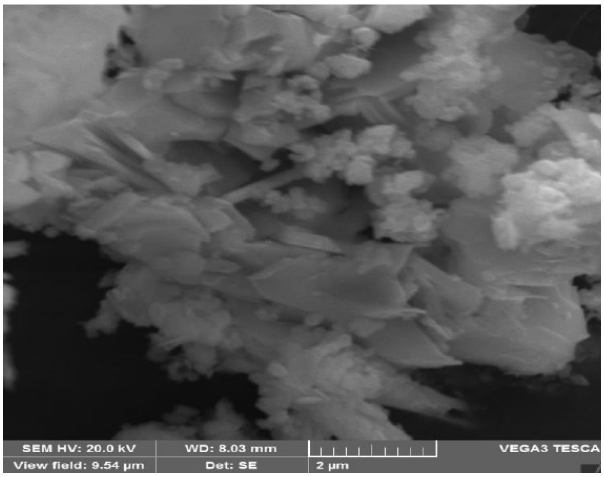

Figure 5c. The FE-SEM image for x=0.01 synthesized sample

Bi-2223 phase for the Bi-2212 and/or Bi-2212+Zr phase. Also, the superconducting transition width (ΔTC) is defined by the difference of T_C^{onset} and T_C^{offset} for each superconductivity phase. So, the obtained

temperatures are shown by arrows for the pure synthesized sample in Figure 6. Also, as shown, all samples display metallic behavior above T_C^{onset} and show that the metallicslope of the synthesized samples decrease with the increase of Zr doping. The obtained transition temperatures of the synthesized samples are listed in Table 4.

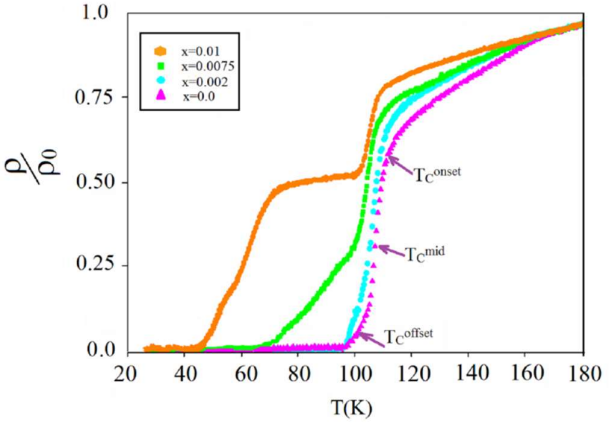

Figure 6. The normalized resistivity versus temperature for synthesized $Bi_{1.66}Pb_{0.34}Sr_2Ca_2Cu_{3-x}Zr_xO_{10+\delta}$ samples (The different supercunducting temperatures shown by arrows for x=0.0).

It is understood that T_C decreases with the increase in the Zr content, and the second superconducting transition is seen for x≥0.0075. Also, the superconducting transition width (ΔT_C) decreases by increasing the Zr doping up to x=0.0075, which can be a consequence of higher homogeneity and shortage of undesirable phases in the mentioned samples according to the results of MAUD analysis in Table 1. As we know, it has been shown that a longer lattice parameter "c" presents a higher T_C in the cuprate superconductors [44, 46]. In the present study, the resistivity results show that the same trend exists between T_C and "c" in the synthesized samples.

The temperature dependence of the normalized resistivity under different magnetic fields (H=0-6.5 kOe) for x=0.0, 0.0075, and 0.01 are presented in Figure 7. It can be found from these graphs that the normal-state behavior of all samples is not changed by applying magnetic fields. In the superconductivity transition region, the applied magnetic fields cause a slight change in the electrical resistivity near the T_C^{onset} that is affiliated with intragrain features. For H> 3kOe, the change in the electrical resistivity near T_C^{onset} is more for the x=0.0075 compound compared to the other samples (see Figure 7b). Also, at lower temperatures,

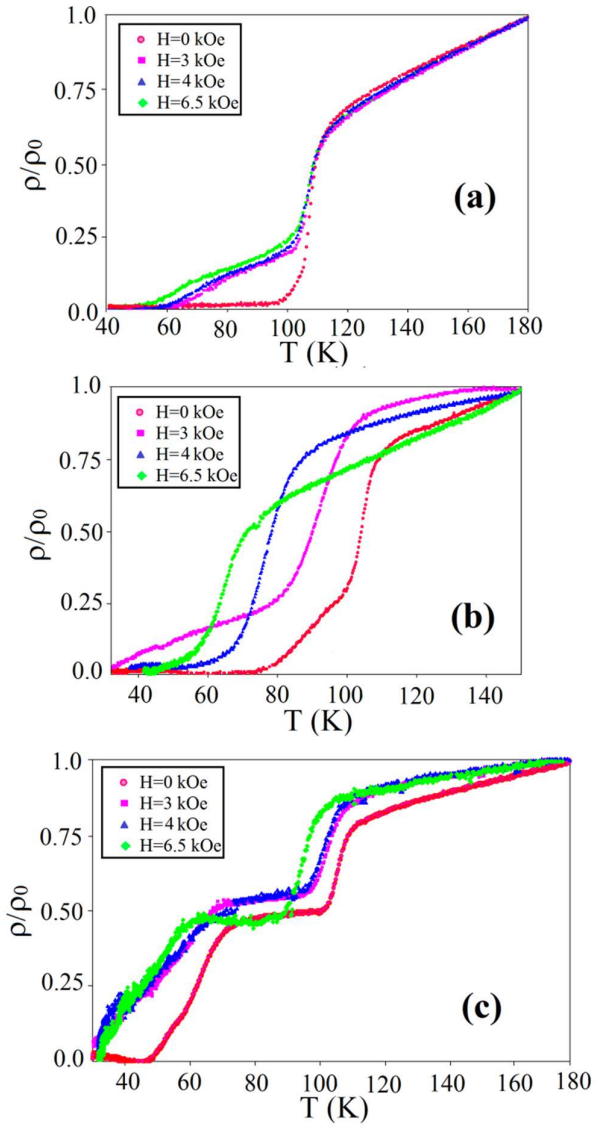

Figure.7. The normalized resistivity for **(a)** the x=0.0, **(b)**x=0.0075, and **(c)**x=0.01 synthesized samples under magnetic fields H=0-6.5 kOe.

applying the magnetic field has a more severe effect on the resistivity curve tail and the superconductivity temperature at ρ = 0 (T_C^{offset}) for all synthesized samples. The intergrain properties of the sample such as defects, weak connections between grains, porosity, etc. can be investigated by the sensitive part to magnetic fields. According to the TAFC model, such behavior can be investigated by the Arrhenius equation [47, 48]:

$$\rho(H.T) = \rho_0 \exp\left(\frac{-U(H)}{k_B\, T}\right), \qquad (3)$$

where, k_B is Boltzmann's constant, ρ_0 is the normal-state resistivity (the resistivity of the superconductors near room temperature), and U(H) is the pinning energy

which can be calculated from the slope of the ln ρ(1/T) plot at superconductivity region. The Arrhenius plots of resistivity for various Zr dopings are shown in Figure 8 with the applied magnetic fields. Accordingly, ρ_0 is a fitting parameter calculated from extrapolation of the ln ρ(1/T) plots so that it varies from 105 to 108 mΩcm. The obtained values are larger than the actual resistivity of the normal state (<8 mΩcm) of the synthesized samples. Similarly, this difference was reported for $Bi_{2.2}Sr_2Ca_{0.8}Cu_2O_{8+\delta}$ [49], $(Y/Gd)_3Ba_5Cu_8O_{18+\delta}$ [34], and $Y_2Ba_5Cu_7O_x$ [33].

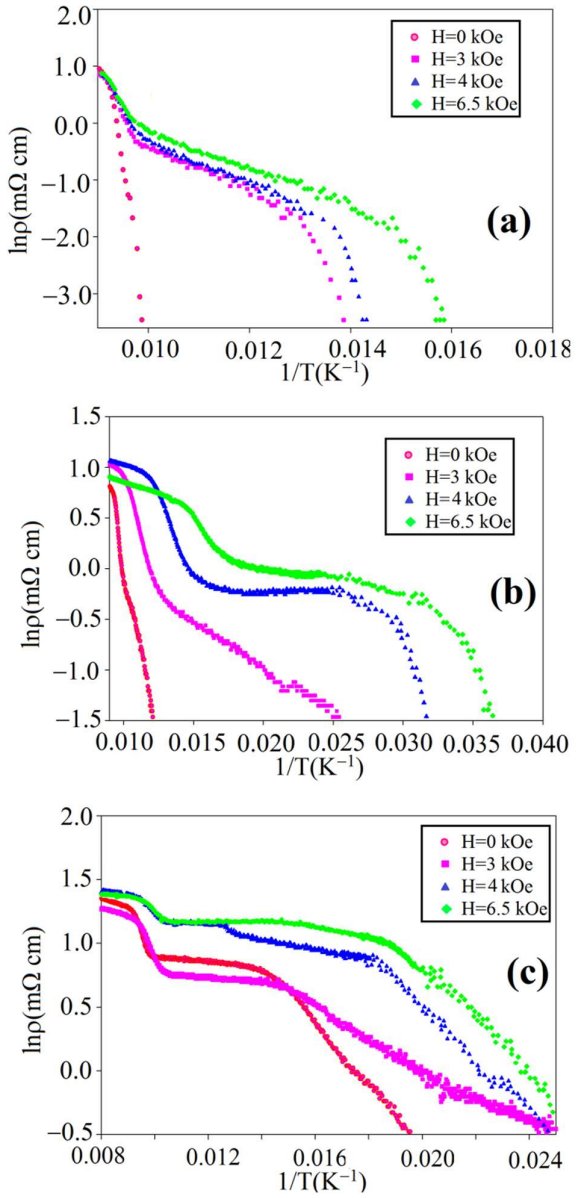

Figure 8. The Arrhenius curves for **(a)** the x=0.0, **(b)** x=0.0075, and **(c)** x=0.01 synthesized samples under magnetic fields H=0-6.5 kOe.

Although there are some reports about the temperature independence of the pinning energy in HTSC [35, 50, 51], our results indicate that the pinning energy of the synthesized samples is affected by magnetic field and temperature. So, variation of the pinning energy with temperature may be studied by the following equation [52]:

$$U = U(H)\left(1 - \frac{T}{T_C}\right)^{\alpha}, \qquad (4)$$

where, α=1, 1.5, and 2 were reported for HTSC [31, 34, 53, 54] and U(H) should be replaced from the result of the Arrhenius plot.

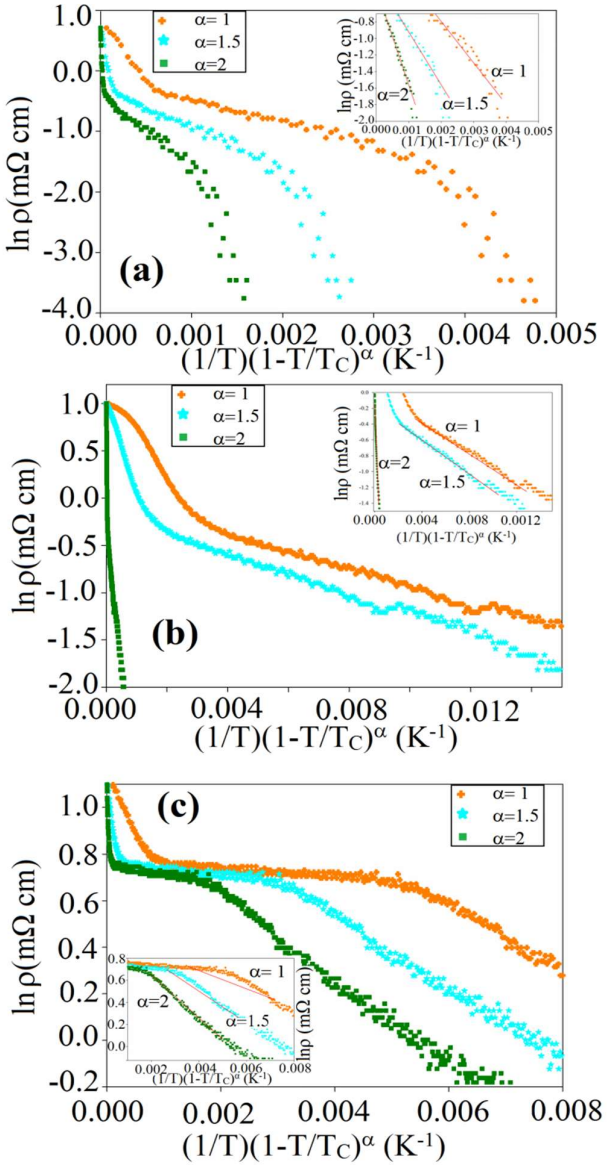

Figure 9. The variation of ln ρ versus $(1/T)(1-T/T_C)^{\alpha}$ for **(a)** the x=0.0, **(b)** x=0.0075, and **(c)** x=0.01 synthesized samples under H=3 kOe.

The best value of α for our synthesized samples is obtained from the dependence of lnρ on $(1/T)(1-T/T_c)^{\alpha}$. The plots for α=1, 1.5, and 2 are displayed in Figure 9 under H=3 kOe. As shown in the inset of these plots, the best fit with the line is obtained for α=2 and this offered that the superconductivity in our samples occurs in two-dimensions. The result is in good agreement with the other cuprates [31, 33, 34].

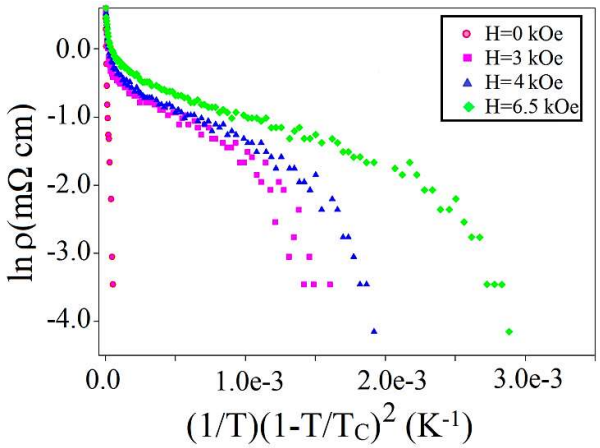

Figure 10. The variation of ln ρ versus $(1/T)(1-T/T_C)^2$ for the x=0.0 synthesized compound under H=3 kOe.

Consequently, Figure 10 shows the curves of lnρ in terms of $(1/T)(1-T/T_c)^2$for the x=0.0 synthesized sample. The pinning energy is calculated from the slope of fitted curves with lines in the tail region. As shown in Figure 11, the pinning energy decreases with increase of the applied magnetic fields for the synthesized samples. Also, the lnρ in terms of $(1/T)(1-T/T_c)^2$curves has been plotted for other Zr dopings, and flux pinning energies have been calculated for the different Zr doping.

Figure 12 shows the flux pinning energy versus the applied magnetic field for the Zr doping and also the inset displays the variation of flux pinning energy against Zr content under H=0 kOe. It is found that the pinning energy remarkably decreased upon increasing the Zr doping and applied magnetic fields. Consequently, the creeping of vortices and crossing the energy barrier due to pinning centers happen more easily and so the pinning energy decreases with the raise of Zr doping compared to the Bi-2223 superconductor.

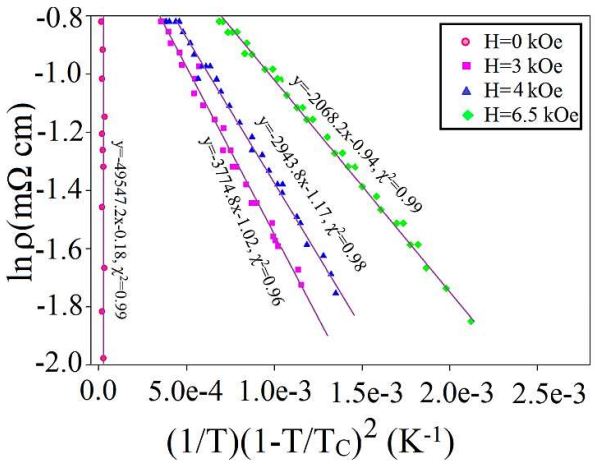

Figure 11. The ln ρ vs. $(1/T)(1-T/T_C)^2$ curves that are fitted with the line under various magnetic fields for x=0.0 synthesized sample.

As mentioned before, the microstrain values of the synthesized samples obtained from the William-Hall method based on the XRD Data (presented in Table 3) have approximately the same values and also, the grains connectivity, defects, orientations, and porosities of the synthesized samples did not noteworthy change based on FESEM measurements with the raise of the Zr doping. Therefore, the reduction of pinning energies can be attributed to the existence and substitution of Zr/Cu ions in the CuO2 planes in grains. These results are in agreement with the reported results in other doped BSCCO compounds [11, 50, 55-57].

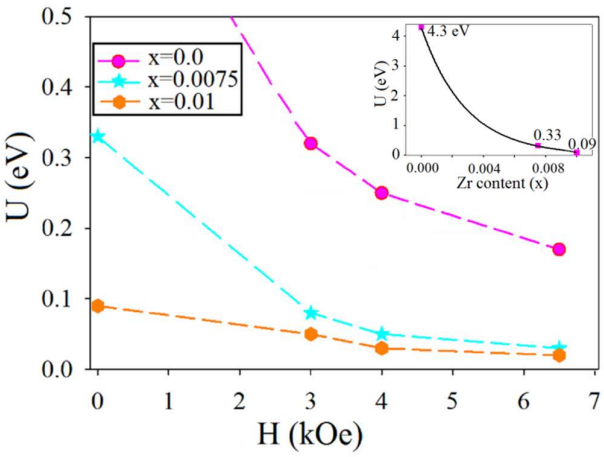

Figure 12. The flux pinning energy versus applied magnetic field for the various Zr dopings samples. Inset is the variation of flux pinning energy against Zr content under H=0 kOe.

Moreover, the pinning energy of the synthesized samples is presented in Figure12. It can be seen the behavior of pinning energies in magnetic fields for our samples is in good agreement with other HTSC. Also,

the pinning energies of our synthesized samples have an equal order of magnitude compared to other HTSC, such as single crystals of $Bi_{2.2}Sr_2Ca_{0.8}Cu_2O_8$ [49], GdPr123 [58], $Bi_2Sr_2Ca_{1-x}Ce_xCu_2O_{8+\delta}$ [50], NaBi-2212 [51], and $Y_{1-x}Tb_xBa_2Cu_3O_{7-\delta}$ [54].

Furthermore, it is advisable to indicate that the most remarkable differences have been observed between the curves in Figure 11 for H≤3 kOe. Also, when the magnetic field rises from 3 to 6.5 kOe, the reduction rate of the pinning energy is softened. It can be suggested that above 3 kOe, the pinning centers are completely occupied by the magnetic field flux in the grains and the Lorentz force will exceed the pinning force in the intergrain regions in the synthesized samples. In other words, the flux creep increases in the intergrain areas by the substitution of Zr/Cu ions in the Bi-2223 superconductor.

4. Conclusions

In this study, we synthesized the $Bi_{1.66}Pb_{0.34}Sr_2Ca_2Cu_{3-x}Zr_xO_{10+\delta}$ ceramic superconductors with x=0.0, 0.002, 0.0075, and 0.01by the sol-gel method. The following results were concluded:

1. Based on the XRD patterns, and MAUD analysis:
   - For x≤0.0075, the Zr doping promoted the stability of the Bi-2223 phase and reduced the undesirable phases in the synthesized samples. So, it seems that a small amount of Zr/Cu substitution (x≤0.0075) can be helpful to remove the undesirable secondary phases in Bi-2223 superconductors. The suggested strategy for the preparation of the Bi-2223 superconductor and the ease usage of the mentioned method can smooth the way toward industrial applications and create a considerable future for this superconductor in high-current systems.
   - The Zr ions preferred to place more in the Bi-2223 phase, and also the Zr/Cu substitution has occurred in the CuO_2 planes.
   - By substitution of Cu ions by Zr ions up to x=0.002, the lattice parameters of the Bi-2223+Zr phase enhanced in comparison to the undoped sample, and "c" reduced with more increasing of the Zr doping. In continued, the lattice parameter "c" declined with the increase of the Zr doping for the Bi-2223 phase.
2. Based on the magnetoresistivity measurements:
   - T_C decreases with increasing the Zr doping and the second superconducting transition occurs for x≥0.0075.
   - By studying the temperature dependence of the pinning energy, using the modified TAFC model obtained an appropriate linear fit in α=2 and it recommends that the superconductivity for synthesized compounds occurs in two dimensions. Also, the pinning energy decreased with raise of the Zr doping in applied magnetic fields. So, the flux creep had happened more easily in the synthesized samples by the substitution of Zr/Cu ions in the Bi-2223 superconductor.

Acknowledgements

The authors are grateful to Vice-Chancellor Research and Technology of Alzahra University for financial support.

References

[1] D. C. Green, R. Boston, S. Glatzel, M. R. Lees, S. C. Wimbush, J. Potticary, W. Ogasawara, S. R. Hall, "On the Mechanism of Cuprate Crystal Growth: The Role of Mixed Metal Carbonates." Advanced Functional Materials, **25** (2015) 4700.

[2] M. Foltyn, S. R. Civale, L. MacManus-Driscoll, J. L. Jia, Q. X. Maiorov, B. Wang, H. Maley, 'Materials science challenges for high-temperature superconducting wire." Nature. Materials, **6** (2007) 631.

[3] M. Pakdil, E. Bekiroglu, M. Oz, N. K. Saritekin, G. Yildirim, "Role of preparation conditions of Bi-2223ceramic materials and optimization of Bi-2223 phase in bulk materials with experimental and statistical approaches." Journal of Alloys and Compounds, **673** (2016) 205.

[4] F. Shahbaz Tehrani, V. Daadmehr, "The superconductivity mechanism in Nd-1111 iron-based superconductor doped by calcium." Journal of Low Temperature Physics, **199** (2020) 1299.

[5] E. Hannachi, M. A. Almessiere, Y. Slimani, A.

Baykal, F. Ben Azzouz, "AC susceptibility investigation of YBCO superconductor added by carbon nanotubes." Journal of Alloys and Compounds, **812** (2020) 152150.

[6] Y. Ding, R. Zhong, J. Schneeloch, G. D. Gu, L. Wang, K. He, S. H. Ji, L. Zhao, X. J. Zhou, C. L. Song, X. C. Ma, Q. K. Xue, Electronic structure of the ingredient planes of the cuprate superconductor $Bi_2Sr_2CuO_{6+\delta}$: A comparison study with $Bi_2Sr_2CaCu_2O_{8+\delta}$, Physical Review B, **93** (2016) 140504(R).

[7] D. Sharma, R. Kumar, V. P. S. Awana, "DC and AC susceptibility study of sol–gel synthesized $Bi_2Sr_2CaCu_2O_{8+\delta}$ superconductor." Ceramics International, **39** (2013) 1143.

[8] H. Fallah-arani, S. Baghshahi, D. Stornaiuolo, F. Tafuri, D. Massarotti, & N. Riahi-noori, "The influence of heat treatment on the microstructure, flux pinning and magnetic properties of bulk BSCCO samples prepared by sol-gel route." Ceramics International, **44** (2018) 5209.

[9] N. Darsono, D. Y. K. Raju, "Effects of the sintering conditions on the structural phase evolution and T_C of $Bi_{1.6}Pb_{0.4}Sr_2Ca_2Cu_3O_7$ prepared using the citrate sol–gel method." Journal of Superconductivity and Novel Magnetism, **29** (2016) 1491.

[10] D. Li, H. Zhang, X. Gao, S. Yang, Q. Chen, "Effect of the fabrication process on the electrical properties of polycrystalline $Bi_{1.7}Pb_{0.3}Sr_2Ca_2Cu_3O_{10}$." Ceramics International, **42** (2016) 1728.

[11] A. Costa, F. M. Ferreira, N. M. Rasekh, S. Fernandes, A. J. S. Torres, M. A. Madre, M. A. Diez, J .C. Sotelo, "Very Large Superconducting Currents Induced by Growth Tailoring." Crystal Growth & Deseign, **15** (2015) 2094.

[12] Y. F. Lv, W. L. Wang, H. Ding, Y. Wang, Y. Ding, R. Zhong, J. Schneeloch, G.D. Gu, L. Wang, K. He, S. H. Ji, L. Zhao, X. J. Zhou, C. L. Song, X. C. Ma, Q. K. Xue, "Electronic structure of the ingredient planes of the cuprate superconductor $Bi_2Sr_2CuO_{6+\delta}$: A comparison study with $Bi_2Sr_2CaCu_2O_{8+\delta}$." Physical Review B, **93** (2016) 140504.

[13] Y. F. Lv, W. L. Wang, J. P. Peng, H. Ding, Y. Wang, L. Wang, K. He, S.-H. Ji, R. Zhong, J. Schneeloch, G. D. Gu, C. L. Song, X. C. Ma, Q. K. Xue, "Mapping the Electronic Structure of Each Ingredient Oxide Layer of High-Tc Cuprate Superconductor $Bi_2Sr_2CaCu_2O_{8+\delta}$." Physical Review Letters, **115** (2015) 237002.

[14] N. Türk, H. Gündoğmuş, M. Akyol, Z.D. Yakinci, A. Ekicibil, B. Özçelik, "Effect of tungsten (W) substitution on the physical properties of Bi-(2223) superconductors." Journal of Superconductivity and Novel Magnetism, **27** (2014) 711.

[15] Y. L. Chen, R. Stevens, "2223 Phase Formation in Bi (Pb)-Sr-Ca-Cu-O: I, The Role of Chemical Composition." Journal of American Ceramic Society, **75** (1992) 1142.

[16] F. H. Chen, H. S. Koo, T. Y. Tseng, "Effect of Ca_2PbO_4 additions on the formation of the 110 K phase in Bi-Pb-Sr-Ca-Cu-O superconducting ceramics." Applied Physics Letters, **58** (1991) 637.

[17] J. Yoo, S. Kim, J. W. Ko, Y. K. Kim, "The fabrication of fine and homogenous Bi-2223 precursor powder by a spray pyrolysis process." Superconductor Science and Technology, **17** (2004) S538.

[18] D. Sharma, R. Kumar, V. P. S. Awana, "DC and AC susceptibility study of sol-gel synthesized $Bi_2Sr_2CaCu_2O_{8+\delta}$ superconductor." Ceramics International, **39** (2013) 1143.

[19] N. Darsono, D. Y. K. Raju, "Effects of the Sintering Conditions on the Structural Phase Evolution and Tc of $Bi_{1.6}Pb_{0.4}Sr_2Ca_2Cu_3O_7$ Prepared Using the Citrate sol – gel Method." Journal of Supercondivity and Novel Magnetism, **29** (2016) 1491.

[20] M. K. Ben Salem, Y. Slimani, E. Hannachi, F. Ben Azzouz M. Ben Salem, "Bi-based superconductors prepared with addition of $CoFe_2O_4$ for the design of a magnetic probe." Cryogenics, **89** (2018) 53.

[21] D. H. Tran, A. T. Pham, T. M. Le, D. T. K. Anh, Y. T. Phan, N. K. Man, D. Pham, W. N. Kang, "Enhanced flux pinning properties in $Bi_{1.6}Pb_{0.4}Sr_{2-x}K_xCa_2Cu_3O_{10+\delta}$ compounds." Journal of Materials Science: Materials in Electronics, **30** (2019) 8233.

[22] B. Özçelik, H. Gundogmus¸D. Yazici, "Effect of (Ta/Nb) co-doping on the magnetoresistivity and flux pinning energy of the BPSCCO superconductors." Journal of Materials Science: Materials in Electronics, **25** (2014) 2456.

[23] G. Kirat, O. Kizilaslan, M. A. Aksan, "Effect of the Er-substitution on critical current density in glass-ceramic $Bi_2Sr_2Ca_2Cu_{3-x}Er_xO_{10+\delta}$ superconducting system." Ceramics International, **42** (2016) 15072.

[24] S. M. Khalil, "Role of rare-earth Ba^{2+} doping in governing the superconducting and mechanical characteristics of Bi-Sr-Ca-Cu-O." Smart Materials and Structure, **14** (2005) 804.

[25] B. Özkurt, "Improvement of the critical current density in Bi-2223 ceramics by sodium-silver co-doping." Journal of Materials Science: Materials in Electronics, **25** (2014) 3295.

[26] R. Wesche, High-Temperature Superconductors: Materials, Properties, and Applications, Springer US, Boston, MA, 1998, pp. 52-70.

[27] K. Neeraj, Handbook of High-Temperature Superconductor, CRC press, New Delhi, 2003, pp. 112-114.

[28] Z. Y. Jia, H. Tang, Z. Q. Yang, Y. T. Xing, Y. Z. Wang, G. W. Qiao, "Effects of nano-ZrO_2 particles on the superconductivity of Pb-doped BSCCO." Physica C, **337** (2000) 130.

[29] M. Zouaoui, A. Ghattas, M. Annabi, F. Ben Azzouz, M. Ben Salem, "Effect of nano-size ZrO_2 addition on the flux pinning properties of (Bi, Pb)-2223 superconductor." Superconductor Science and Technology, **21** (2008) 125005.

[30] H. Azhan, F. Fariesha, S. Khalida, "Effect of Heat Treatments and Zr Doped on Superconducting Properties of $Bi_{1.6}Pb_{0.4}Sr_2Ca_2Cu_3O_\delta$ Ceramics." Journal of Supercondivity and Novel Magnetism, **24** (2011) 265.

[31] A. Heidari, S. Vedad, N. Heidari, M. Ghorbani, "Flux Dynamics in Y358 Superconductors." Materials, **5** (2012) 882.

[32] S. Vinu, P. M. Sarun, R. Shabna, P. M. Aswathy, J. B. Anooja, U. Syamaprasad, "Suppression of flux-creep in (Bi,Pb)-2212 superconductor by holmium doping." Physica B, **405** (2010) 4355.

[33] M. Mazaheri, S. Jamasb, "Electrical transport in the superconducting and normal states in $Y_2Ba_5Cu_7O_x$ high-temperature superconductor." Solid State Commuications, **234** (2016) 21.

[34] A. Aliabadi, Y. Akhavan-Farshchi, M. Akhavan, Flux Dynamics in Y358 and Gd358 Superconductors, Journal of Supercondivity and Novel Magnetism, **27** (2014) 741.

[35] H. Gündoğmuş, B. Özçelik, A. Sotelo, M. A. Madre, "Effect of Yb-substitution on thermally activated flux creep in the $Bi_2Sr_2Ca_1Cu_{2-x}Yb_xO_y$ superconductors." Journal of Materials Science: Materials in Electronics, **24** (2013) 2568.

[36] D. Ahmad, W. J. Choi, Y. I. Seo, SehunSeo, Sanghan Lee, Yong Seung Kwon, "Thermally activated flux flow in superconducting epitaxial $FeSe_{0.6}Te_{0.4}$ thin film." Results in Physics, **7** (2017) 16.

[37] M. Tinkham, "Resistive transition of high-temperature superconductors." Physical Review Letters, **61** (1988) 1658.

[38] M. R. Mohammadizadeh, M. Akvahan, "Magnetoresistance in $Gd(Ba_{2-x}Pr_x)Cu_3O_{7+\delta}$ system." Physica C, **390** (2003) 134.

[39] Y. Zalaoglu, G. Yildirim, C. Terzioglu, "Magnetoresistivity study on Cr added Bi-2212 superconductor ceramics with experimental and theoretical approaches." Journal of Materials Science: Materials in Electronics, **24** (2013) 239.

[40] M. B. Turkoz, S. Nezir, A. Varilci, G. Yildirim, M. Akdogan, C. Terzioglu, "Experimental and theoretical approaches on magnetoresistivity of Lu-Doped Y-123 superconducting ceramics."

Journal of Materials Science: Materials in Electronics, **24** (2013) 1536.

[41] F. Shahbaz Tehrani, V. Daadmehr, "Superconductivity Versus Structural Parameters in Calcium-Doped Nd1-xCaxFeAsO0.8F0.2 Superconductors." Journal of Supercondivity and Novel Magnetism, **33** (2020) 337.

[42] O. Özturk, D. Yegen, M. Yilmazlar, A. Varilci, C. Terzioglu, "The effect of cooling rates on properties of $Bi_{1.7}Pb_{0.35}Sr_{1.9}Ca_{2.1}Cu_3O_y$ superconductors produced by solid-state reaction method." Physica C Superconductivity and its Applications, **451** (2007) 113.

[43] N. Darsono, D. Y. K. Raju, Effects of the Sintering Conditions on the Structural Phase Evolution and Tc of Bi1.6Pb0.4Sr2Ca2Cu3O7 Prepared Using the Citrate sol – gel Method, Journal of Supercondivity and Novel Magnetism, **26** (2016) 1491.

[44] N. Zarabini, V. Daadmehr, F. Shahbaz Tehrani, M. Abbasi, "Influence of Ag/Cu Substitution on Structural Effect of New High Temperature Superconductor Y3Ba5Cu8O18." Procedia Materials Science, **11** (2015) 242.

[45] G. K. Williamson, W. H. Hall, Acta Metallurjica, **1** (1953) 22.

[46] S. Karimoto, H. Yamamoto, H, Sato, A. Tsukada, M. Naito, "T_C versus lattice constants in MBE-grown M_2CuO_4 (M=La, Sr, Ba)." Journal of Low Temperature Physics, **131** (2003) 619.

[47] W. J. Choi, D. Ahmad, Y. I. Seo, R. K. Ko,Yong Seung Kwon, Effect of the proton irradiation on the thermally activated flux flow in superconducting SmBCO coated conductors, Scientific Reports, **10** (2020) 2017.

[48] R. Gross, P. Chaudhari, D. Dimos, A. Gupta, G. Koreu, Thermally activated phase slippage in high-T_C grain-boundary Josephson junctions, Physical Review Letters, **64** (1990) 228.

[49] T. T. M. Palstra, B. Batlogg, R. B. van Dover, L. F. Schneemeyer, J. V. Waszczak, "Dissipative flux motion in high-temperature superconductors." Physical Review B, **41** (1990) 6621.

[50] B. Özçelik, C. Kaya, H. Gundogmus, A. Sotelo, M. A. Madre, "Effect of Ce Substitution on the Magnetoresistivity and Flux Pinning Energy of the $Bi_2Sr_2Ca_{1-x}Ce_xCu_2O_{8+\delta}$ Superconductors." Journal of Low Temperature Physics, **174** (2014) 136.

[51] B. Özçelik, M. Gursul, A. Sotelo, M. A. Madre, Improvement of the Intergranular Pinning Energy in the Na-doped Bi-2212 Superconductors, Journal of Materials Science: Materials in Electronics, **26** (2015) 2830.

[52] T. T. M. Palstra, B. Batlogg, L. F. Schneemeyer, J. V. Waszczak, "Role of anisotropy in the dissipative behavior of high-temperature superconductors." Physical Review B, 43 (1991) 3756.

[53] Y. Sun, S. Pyon, T. Tamegai, R. Kobayashi, T. Watashige, Sh. Kasahara, Y. Matsuda, T. Shibauchi, "Critical current density, vortex dynamics, and phase diagram of single-crystal FeSe." Physical Review B, **92** (2015) 144509.

[54] S. Mirshamsi, S. Fallahi, M. Akhavan, Superconducting properties of $Y_{1-x}Tb_xBa_2Cu_3O_{7-\delta}$ and $Y_{1-x}Tb_xSr_2Cu_{2.7}Mo_{0.3}O_{7-\delta}$, Modern Physics Letters B, **24** (2010) 419.

[55] B. Özçelik, B., M. Gürsul, M., F. K. Nane, M. A. Madre, A. Sotelo, "Effect of Na-substitution on magnetoresistance and flux pinning energy of Bi-2212 ceramics prepared via hot-forging process." Journal of Materials Science: Materials in Electronics, **29** (2018) 19147.

[56] B. Özkurt, B. Özçelik, Effect of Nd-Substitution on Thermally Activated Flux Creep in the Bi1.7Pb0.3−xNdxSr2Ca3Cu4O12+y Superconductors. Journal of Low Temperature Physics, **156** (2009) 22.

[57] B. Özçelik, E. Yalaz, M. E. Yakinci, A. Sotelo, M. A. Madre, "The Effect of K Substitution on Magnetoresistivity and Activation Energy of Bi-2212 System." Journal of Supercondivity and Novel Magnetism, **28** (2015) 553.

[58] V. Daadmehr, M. Akhavan, "Proton Irradiation Effects on Granular High-T_C Superconductors: $Gd_{1-x}Pr_xBa_2Cu_3O_{7-\delta}$." Physica Status Solidi (a). **193** (2002) 153.